Regular Article

Development of a Membrane Curvature-Sensing Peptide Based on a Structure–Activity Correlation Study

Kenichi Kawano, Masaya Ogushi, Toshihiro Masuda, and Shiroh Futaki*

Institute for Chemical Research, Kyoto University; Uji, Kyoto 611–0011, Japan.
Received June 6, 2019; accepted July 10, 2019; advance publication released online July 17, 2019

Membrane curvature formation is important for various biological processes such as cell motility, intracellular signal transmission, and cellular uptake of foreign substances. However, it remains still a challenging topic to visualize the membrane curvature formation on the cell membranes in real-time imaging. To develop and design membrane curvature-sensors, we focused on amphipathic helical peptides of proteins belonging to the Bin/Amphiphysin/Rvs (BAR) family as the starting point. BAR proteins individually have various characteristic structures that recognize different curvatures, and the derived peptides possess the potential to function as curvature sensors with a variety of recognition abilities. Peptide-based curvature sensors can have wide applications in biological research fields due to their small size, easy modification, and large production capability in comparison to protein-based sensors. In the present study, we found that an amphipathic peptide derived from sorting nexin1 (SNX1) has a curvature-recognition ability. The mutation studies of the initial peptide revealed a close correlation between the α-helicity and lipid binding ability of the peptides. In particular, the amino acids located on the hydrophobic face played a vital role in curvature recognition. The α-helix formation of the peptides was thought to serve to accommodate lipid-packing defects on the membrane surface and to maintain their binding to lipid vesicles. The structure–activity correlation found in this study have the potential to contribute to the design of peptide-based curvature sensors that will enable the capture of various life phenomena in cells.

Key words curvature-sensing peptide; amphipathic α-helix; membrane curvature; lipid packing defect; negatively charged lipid

Introduction

Living cell membranes have a surface structure enriched in local asperities, and membrane curvature formation is involved in the processes of cell motility control,[1] intracellular signal transmission,[2] Alzheimer's disease,[3] and cellular uptake of foreign substances.[4,5] Our laboratory has reported a membrane curvature-inducing peptide, EpN18, which has the ability to induce positive membrane curvature accompanied by loosening of lipid packing on the cell membrane.[4,5] Using EpN18, we revealed that lipid-packing loosening is a key factor in facilitating the membrane permeation of arginine-rich cell penetrating peptides. However, it was unclear at what size and timing the curvature was formed by EpN18. In the present study, to visualize the membrane curvature formation on the cell membranes in real-time imaging, we attempted to develop a prototype of the curvature-sensing peptide. In designing the sensor peptide, we focused on well-studied curvature-recognizing proteins with Bin/Amphiphysin/Rvs (BAR) domains. At present, 70 or more types of BAR proteins have been identified *in vivo*, and the proteins that localize to various subcellular organelles such as the endoplasmic reticulum, Golgi apparatus, mitochondria, and endosomes are reported to individually have various characteristic structures that recognize different curvatures.[6] Therefore, peptides derived from amphipathic regions of proteins belonging to the BAR family have the potential to become curvature sensors with a variety of curvature-recognition abilities. Peptide-based sensor tools have an advantage of having wide applications in biological research fields due to their small size, easy modification, and capable of large-scale production capability.

Several curvature-sensing peptides have been reported previously. The effector domain of myristoylated alanine-rich C-kinase substrate (MARCKS-ED), which is known as a curvature and phosphatidylserine (PS) sensing peptide, binds to highly curved vesicles *via* electrostatic interaction with PS lipids.[7] The ArfGAP1 lipid packing sensor (ALPS) motif responds to membrane curvature, inserting bulky hydrophobic residues into sites with loosely packed lipids.[8] The former peptide (25 a.a.) does not have any secondary structure in the presence of vesicles,[7] and its vesicle binding ability is affected by a balance between the positions and numbers of positively charged residues and hydrophobic anchoring residues in its primary structure.[9] The latter one forms an amphipathic helix on the curved membranes but is a highly hydrophobic peptide with a length of 40 a.a., which was defined in the original paper.[8] Inspired by these previous studies, we attempted to create curvature-sensing peptides shorter than 25 residues in length with high water-solubility. Concomitantly with the achievement of our main goal, it was also necessary to investigate the correlation between structural features of the peptides and their curvature recognition abilities. The initial peptides were selected from previously reported α-helical regions of BAR proteins.[10–18]

The peptides derivate from sorting nexin 1 (SNX1) and arfaptin 2 (ARF) were found to have membrane curvature recognition potential at the initial screening. After inducing mutations of the amino acids located on the hydrophobic face of SNX1, the propensity to form α-helices was significantly improved, accompanied by an increase in lipid binding ability. While the SNX1-derived peptide, named FAAV, was unstruc-

* To whom correspondence should be addressed. e-mail: futaki@scl.kyoto-u.ac.jp

© 2019 The Pharmaceutical Society of Japan

tured in solution, it inserted the hydrophobic residues into the lipid-packing defects, followed by formation of an amphipathic α-helix on highly curved membranes. FAAV generated in this study is expected to be a promising prototype of curvature sensors that will enable the capture of life phenomena.

Experimental

Materials For the peptide synthesis, the following reagents were prepared. Fmoc (=9-fluorenylmethyloxycarbonyl)-protected amino acids were purchased from Peptide Institute (Osaka, Japan) and Watanabe Chemical Industries (Hiroshima, Japan). Rink amide resin (TentaGel S RAM) was gained from HiPep Laboratories (Kyoto, Japan). 1-Hydroxybenzotriazole (HOBt), 1-[Bis(dimethylamino)-methylene]-1*H*-benzotriazolium 3-oxide hexafluorophosphate (HBTU), and 1-[Bis(dimethylamino)methylene]-5-chloro-1*H*-benzotriazolium 3-oxide hexafluorophosphate (HCTU) were purchased from Peptide Institute. Trifluoroacetic acid (TFA), 1,2-ethantithiol (EDT), and *N*,*N*-diisopropylethylamine (DIEA) were bought from Watanabe Chemical Industries, Tokyo Chemical Industry (Tokyo, Japan), and FUJIFILM Wako Pure Chemical Corporation (Osaka, Japan), respectively. 4-Fluoro-7-nitrobenzofurazan (NBD-F) was purchased from Dojindo Molecular Technoligies (Kumamoto, Japan).

For the liposome preparation, 1-palmitoyl-2-oleoyl-*sn*-glycero-3-phosphocholine (POPC) and 1-palmitoyl-2-oleoyl-*sn*-glycero-3-phosphoethanolamine (POPE) were bought from NOF corporation (Tokyo, Japan), and 1-palmitoyl-2-oleoyl-*sn*-glycero-3-phospho-L-serine (POPS) and cholesterol were purchased from Avanti Polar Lipids (AL, U.S.A.) and Merck Millipore Japan (Tokyo, Japan), respectively. ANTS (=8-aminonaphthalene-1,2,3-trisulfonic acid) and DPX (=*p*-xylene-bis-pyridinium bromide) were from Merck Millipore Japan, respectively.

Peptide Synthesis Peptides were constructed using a PSSM-8 peptide synthesizer (Shimadzu, Kyoto, Japan), using Fmoc solid phase peptide chemistry on a Rink amide resin.[19] A coupling system using HBTU/HOBt/DIEA was employed. For the synthesis of peptides containing α-aminoisobutyric acid (Aib), HCTU was used as a condensing agent instead of HBTU. In the case of Ahx-MAR (Ahx: ε-aminohexanoic acid), after the introduction of Ahx at the N-terminus onto the peptide resin, the amino group of Ahx was labeled with NBD-F dye (2.5 eq.) and incubated for 24 h at 25°C.[20] For the peptides bearing a NBD moiety on the C-termini, peptide chains were constructed using Lys(Mtt) (Mtt = 4-methyltrityl) for C-terminal Lys residues subjected to NBD labeling, and Lys(Boc) for the other Lys residues. After peptide chain construction, N-termini were masked with Boc groups using di-*tert*-butyl dicarbonate (Boc_2O) in the presence of *N*-methylmorpholine/dimethylformamide (1 : 49)(1.5 h at 25°C). The Mtt group was then selectively removed on resin by incubation with hexafluoroisopropanol/dichloromethane (1 : 4) for 3 h at 25°C,[21] prior to treatment with NBD-F (2.0 eq.) for 24 h at 25°C.[20] The final deprotection of the peptides and the cleavage from the resin were conducted using TFA/EDT (95 : 5) at 25°C for 3 h.

The peptides were purified by reverse-phase (RP)-HPLC on COSMOSIL $5C_{18}$-AR-II or $5C_4$-AR-300 columns (10ID × 250 mm) (Nacalai Tesque, Kyoto, Japan), followed by lyophilization. The masses of the products were confirmed by matrix-assisted laser desorption ionization time-of-flight MS (Bruker Daltonics Japan, Yokohama, Japan) (Supplementary Table S1). The purified peptides were dissolved in phosphate-buffered saline [PBS(–): 137 mM NaCl, 2.7 mM KCl, 10 mM Na_2HPO_4, and 1.8 mM KH_2PO_4] for use in experiments. The concentrations of the dye-labeled peptides were calculated by measurement of the NBD absorption at 467 nm ($\varepsilon = 28{,}000\,cm^{-1}M^{-1}$). The concentrations of non-labeled peptides without the linkers used for circular dichroism (CD) spectra measurement were estimated based on weight.

Liposome Preparation For preparation of liposomes with the standard lipid composition, POPC, POPE, cholesterol and POPS were mixed with the molar ratio of 60 : 15 : 15 : 10 in chloroform in an eggplant flask, and evaporated for 30 min followed by vacuum drying for 12 h, finally yielding a lipid film on the inside surface of the flask. The lipid film was gently hydrated for 1 h at 25°C with occasional vortexing to prepare a liposome solution. To control the size of liposomes, a LyposoFast extrusion system (Avestin, Mannheim, Germany) and Whatman polycarbonate (PC) filters (GE Healthcare Japan, Tokyo, Japan) with pore sizes of 200, 100, 50 nm and 30 nm were used. A PC filter was attached to the LyposoFast extrusion system, and the size of liposomes was adjusted by passing 21 times through the PC filter. When preparing lipid vesicles of 120 nm in diameter, a PC filter with a pore size of 200 nm was used. When preparing lipid vesicles of 50 nm in diameter, PC filters with pore sizes of 200, 100, 50, and 30 nm were used sequentially.

The concentrations of the lipid vesicles were determined following the protocol of the LabAssay Phospholipid Kit (FUJIFILM Wako Pure Chemical Corporation). The lipid vesicles were stored at 4°C, and used within 3 d after preparation.

The particle sizes of the lipid vesicles were determined by dynamic light scattering. Measurement was done at 25°C at a liposome concentration of 1 mM in PBS(–) by using a Zetasizer Nano ZS (Malvern Panalytical, Worcestershire, U.K.) with a scattering angle of 173°.

Evaluation of Lipid Vesicle Binding of Peptides The NBD-labeled peptides (0.5 μM) and lipid vesicles of 50 or 120 nm in diameter (0.5 mM) were mixed together in PBS(–) and incubated for 1 h at 25°C. The fluorescence intensity of the NBD dye was measured using a Wallac 1420 Victor2 Microplate Reader (PerkinElmer, Inc., Japan, Yokohama, Japan) at an excitation wavelength of 485 nm and a fluorescence wavelength of 535 nm. The measured fluorescence intensities were expressed in terms of relative fluorescence intensity (RFI) with the fluorescence intensity of each peptide alone described as "Peptide only" in the Figs. 1, 2, and 4.

Measurement of CD Spectra Non-labeled peptides without the linker segments were used for the measurement of CD spectra (Supplementary Table S1). Non-labeled peptides (20 μM) and lipid vesicles of 50 or 120 nm in diameter (2 mM) were mixed together in PBS(–) and incubated for 1 h at 25°C. The measurement of CD spectra was performed using a J-820 circular dichroism spectrometer (JASCO, Tokyo, Japan).

Leakage Assay In the leakage assay, the lipid film was hydrated in the presence of 12.5 mM ANTS (a fluorescent dye) and 45 mM DPX (a quencher). After repeating five freeze-thaw cycles, the liposomes were extruded following the same protocol used for liposome preparation to obtain lipid vesicles of 50 or 120 nm in diameter. The concentrations of lipid vesi-

cles were fixed at 0.4 mM and the lipid/peptide ([L]/[P]) ratio was varied (1500, 600, 100, and 10). The fluorescent intensity of ANTS dye was measured at an excitation wavelength of 355 nm and emission of 535 nm using a Wallac 1420 Victor2 Microplate Reader after incubation of lipid vesicles with the peptides for 1 h at 25°C. Then, Triton X-100 was added to the sample solution at a final concentration of 0.1% (v/v) and incubated for 15 min at 37°C. The fluorescence intensity of ANTS dye was then measured again.

Results

Screening of Curvature-Sensing Peptides To evaluate the structural features of curvature-sensing peptides, we chose various sequences as the initial peptides.[10–18] The selected peptides were derived from amphipathic regions of proteins from each phylogenetic group of the BAR-domain family.[22] The corresponding peptides were prepared by Fmoc solid phase synthesis (Table 1). The peptides, including linker segments, were all adjusted to the same length to evaluate curvature recognition under the same conditions; if the lengths differ, longer peptides have an enthalpy advantage for forming helical structures, which could be a factor in curvature sensing. The Lys residue located at the C-terminus of the peptides was labeled with NBD, a dye that strongly emits fluorescence in hydrophobic environments such as membranes. The labeling site was distanced from curvature-sensing regions *via* a GSGS linker to avoid effects on liposome binding. MARCKS-ED was used as a control, because it has already been established as a curvature sensor and has a similar length (25 residues) to the candidate amphipathic peptides (23 residues); the only difference is that MARCKS-ED forms no secondary structure when bound to microvesicles. Two types of MARCKS-ED with different labeling sites were prepared here. One was the original peptide, labeled at the N-terminus *via* an Ahx linker.[7] The other had a labeling site at the C-terminus, like the amphipathic peptides. The amphipathic peptides with NBD labeling at the N-termini were not prepared here because the N-termini were reported to be important for curvature recognition.[13] A liposome binding system was ideal for evaluation of the curvature recognition capability of the peptides for the following reasons; (*i*) peptide binding sites exist throughout the entire surface due to the spherical shape with high curvature; (*ii*) the vesicle sizes (*i.e.*, degree of membrane curvature), lipid composition, and lipid type can be easily changed, and (*iii*) the factors influencing the binding ability of peptides can be confirmed one by one. As a lipid model of the plasma membranes of mammalian cells, the liposomes used here were composed of POPC, cholesterol, POPE, and POPS at 60, 15, 15, and 10 mol%, respectively.[23–25] Two types of liposomes with the same lipid compositions but different sizes (curvatures) were prepared. The diameters of the liposomes determined by dynamic light scattering were 48 ± 12 and 120 ± 42 nm (mean ± standard deviation (S.D.), $n = 10$), hereafter, referred to as 50 nm and 120 nm vesicles, respectively. For peptides with a curvature-sensing capacity, the NBD dye conjugated to the peptide should emit higher fluorescence intensity in the presence of 50 nm vesicles with higher curvature in comparison to the 120 nm vesicles with lower curvature.

Table 1. Amino Acid Sequences of Peptides Derived from Proteins of the BAR Domain Family[a]

Peptide	Sequence (X = Norleucine, Ahx = ε-Aminohexanoic acid)
Ahx-MAR	NBD-Ahx-KKKKKRFSFKKSFKLSGFSFKKNKK-amide
MAR	KKKKKRFSFKKSFKLSGFSFKKNKK-GSGSK(NBD)-amide
END	SVAGLKKQFHKATQKVSE-GSGSK(NBD)-amide
AMP	FAKNVQKRLNRAQEKVLQ-GSGSK(NBD)-amide
NDR	XKKQFNRXKQLANQTVGR-GSGSK(NBD)-amide
BRAP	AAGLFAKQVQKKFSRAQE-GSGSK(NBD)-amide
PICK	SLDIVLKKVKHRLVENXS-GSGSK(NBD)-amide
SNX1	GAGLLKXFNKATDAVSKX-GSGSK(NBD)-amide
SNX2	GAGILRXVNKAADAVNKX-GSGSK(NBD)-amide
SNX4	TGFQLKADSRLKALNATF-GSGSK(NBD)-amide
ARF	FDIVKKWGINTYKCTKQL-GSGSK(NBD)-amide
OP	XGHPPLEFSDCYLDSPDF-GSGSK(NBD)-amide
CB	SPRFRAALEEVEGDVAEL-GSGSK(NBD)-amide

a) MAR: position 151–175 of the effector domain of myristoylated alanine-rich C-kinase substrate (MARCK-ED)[7,9]; END: position 2–19 of rat endophilin A1[10–14]; AMP: position 9–26 of rat amphiphysin 1[10,11,14]; NDR: position 1–18 of mouse nadrin 2[10,11,15]; BRAP: position 9–26 of homo sapiens BRCA1-associated protein[11]; PICK: positon 113–130 of homo sapiens protein interacting with C-kinase 1[10,11,16]; SNX1, 2, 4: positions 281–298, 278–295, and 194–211 of homo sapiens sorting nexin 1, 2, and 4, repsctively[11,17,18]; ARF: position 93–110 of homo sapiens arfaptin 2[10,11,16]; OP: position 1–18 of homo sapiens oligophrenin 1[10,11]; CB: position 14–31 of homo sapiens centaurin β2.[10,11] In the peptide sequence, the single letter X and triple letters Ahx indicate norleucine and ε-aminohexanoic acid, respectively. The norleucine was used instead of methionine in order to prevent the oxidation effect. The C-termini of all peptides were amidated.

Figure 1 shows the relative fluorescence intensities (RFIs) of NBD-labeled peptides in the presence of two types of lipid vesicles with different curvatures (50 or 120 nm diameter). An increase in the RFI indicates that the peptide bound to the lipid vesicle surface because NBD is a hydrophobic environment-sensitive dye. The fluorescence intensity of each peptide alone was used as the standard, described as "Peptide only." In Fig. 1A, SNX1, SNX2, and ARF showed the same level of RFI as the control, Ahx-MAR. In the presence of 50 nm vesicles, the RFI of these four peptides were 2.5–2.8 (black bars). By contrast, the RFI levels of peptides incubated with 120 nm vesicles (white bars) were lower than those when incubated with 50 nm vesicles. The RFI ratio of each peptide in the presence of 50 and 120 nm vesicles was then obtained to investigate the curvature-sensing abilities of the peptides (Fig. 1B). The SNX1, SNX2, and ARF peptides exhibited average values of 1.57, 1.33 and 1.27, respectively. The control peptides, Ahx-MAR and MAR, exhibited average values of 1.41 and 1.49, respectively. These results indicated that SNX1, SNX2, and ARF also bound the membranes in curvature-dependent manner, and especially SNX1 peptide had the highest curvature-recognition ability among the other peptides. CD spectra of the peptides in the presence of 50 and 120 nm vesicles were given in Supplementary Fig. S1 (SNX2 is not shown). The molar ellipticities at 222 nm ($[\theta]_{222}$) has been used as an indicator of α-helicity. The $[\theta]_{222}$ of SNX1 and ARF in the presence of 50 nm vesicles were slightly lower compared to the others, indicating that these two peptides have a higher helix-forming propensity upon binding to lipid vesicles than the other peptides.

Negatively Charged Lipids Are Important for Peptide Binding to Smaller Lipid Vesicles The surfaces of cancer cells and exosomes are relatively enriched in negatively charged lipids, and PS in particular is externalized to the outer leaflet during canceration.[26,27] With respect to their applications in the elucidation of cancer cell movement and metas-

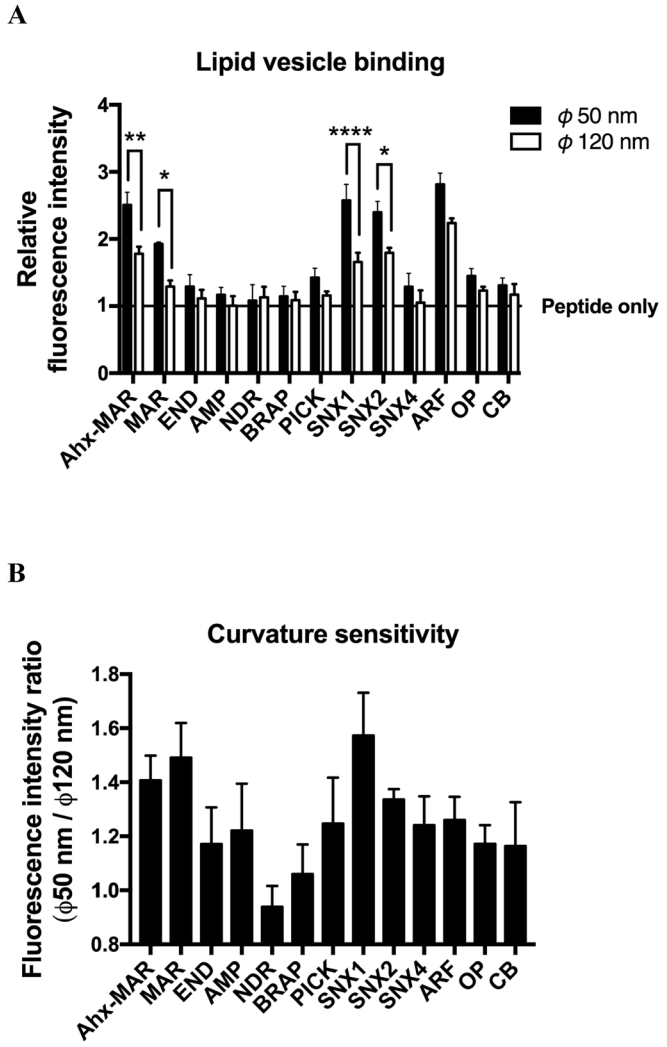

Fig. 1. Screening of the Initial Peptides Derived from Bin/Amphiphysin/Rvs (BAR) Proteins

(A) Comparison of lipid vesicle binding of the peptides. The fluorescence intensity of each peptide alone was normalized ("Peptide only," horizontal solid line), and the relative fluorescence intensity (RFI) on the *y*-axis is the ratio between the fluorescence intensity of peptides with and without incubation with lipid vesicles. The RFI values were measured in the presence of vesicles of either 50 nm (black) or 200 nm (white) in diameter. The lipid/peptide ([L]/[P]) ratio was 1000, and the vesicles were composed of 60 mol% POPC, 15 mol% cholesterol, 15 mol% POPE, and 10 mol% POPS. The data represent mean ± standard error (S.E.) ($n = 4$). (B) Comparison of curvature sensitivity. The fluorescence intensity of each peptide in the presence of 50 nm vesicles was divided by that in the presence of 120 nm vesicles. The data represent mean ± S.E. ($n = 4$). Statistical significance between 50 nm and 120 nm vesicles was determined using Holm–Šídák method of the multiple *t*-test, with $\alpha = 0.05$ (Prism 7, ver. 7.0a software). The results were given in Fig. 1A.

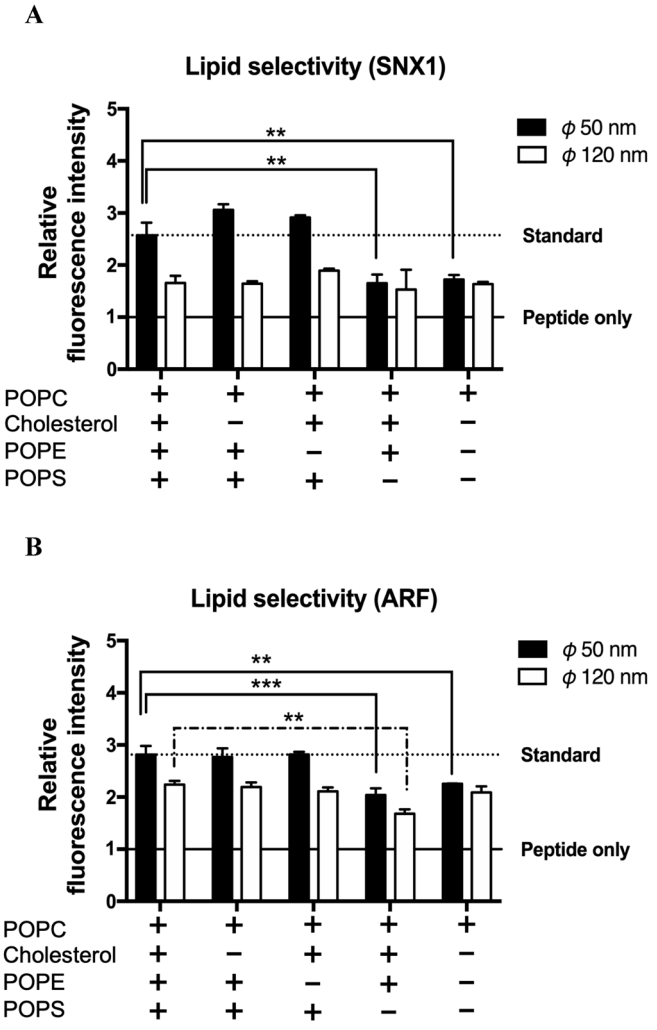

Fig. 2. Evaluation of Lipid Selectivity of SNX1 and ARF

The RFI values of SNX1 (A) and ARF (B) in the presence of vesicles with various lipid compositions were compared. In each panel, the first column on the left shows the standard lipid composition of 60 mol% POPC, 15 mol% cholesterol, 15 mol % POPE, and 10 mol% POPS. The composition of the second column, cholesterol(–), was 75 mol% POPC, 15 mol% POPE, and 10 mol% POPS; the third column, POPE(–), was 75 mol% POPC, 15 mol% cholesterol, and 10 mol% POPS; and the fourth column, POPS(–), was 70 mol% POPC, 15 mol% cholesterol, and 15 mol% POPE. The lipid composition of the final column was 100 mol% POPC. The [L]/[P] ratio was fixed at 1000 in all experiments. The data represent mean ± S.E. ($n = 3$). Statistical significance was determined using the two-way ANOVA Dunnett's and Šídák's multiple comparisons tests, with $\alpha = 0.05$ (Prism 7, ver. 7.0a software).

tasis mechanisms, the negatively charged lipid selectivity of SNX1 and ARF was examined in addition to their membrane curvature recognition. SNX2 was not tested here because its sequence was similar to SNX1 (Table 1) and its vesicle binding and/or curvature sensitivity was lower than SNX1 (Fig. 1). The standard composition of lipid vesicles was the same as in Fig. 1, with POPC, cholesterol, POPE, and POPS at 60, 15, 15, and 10 mol%, respectively (Fig. 2, leftmost bars in each panel). To examine the lipid selectivity of the peptides, additional vesicles were prepared in which various lipids were excluded (*i.e.*, exclusion of cholesterol, POPE, POPS, or all except for POPC). The excluded lipids were replaced with additional POPC, because POPC commonly exists in lipid environments and a larger quantity should not impact the peptide binding. For example, in the second condition from the left in Fig. 2, cholesterol(–), the lipid composition was POPC, POPE, and POPS at 75, 15, and 10 mol%, respectively. The [L]/[P] ratio was fixed at 1000 in all experiments. The RFI values when various lipids were excluded were compared to those of SNX1 (Fig. 2A) and ARF (Fig. 2B) in the presence of 50 nm vesicles with the standard lipid composition (a dashed line).

In comparison with the standard, the RFI values of SNX1 and ARF incubated with 50 nm vesicles fell in the absence of POPS, while in the absence of cholesterol or POPE the RFI values did not drop (Fig. 2, black bars). With POPC only, the RFI values of SNX1 and ARF decreased to the same level observed with the exclusion of POPS alone (Fig. 2, rightmost bars in each panel). By contrast, when the peptides were incubated with 120 nm vesicles, the RFI values remained almost the same level as the standard both in the absence of POPS and with POPC only (Fig. 2, white bars). This suggested that

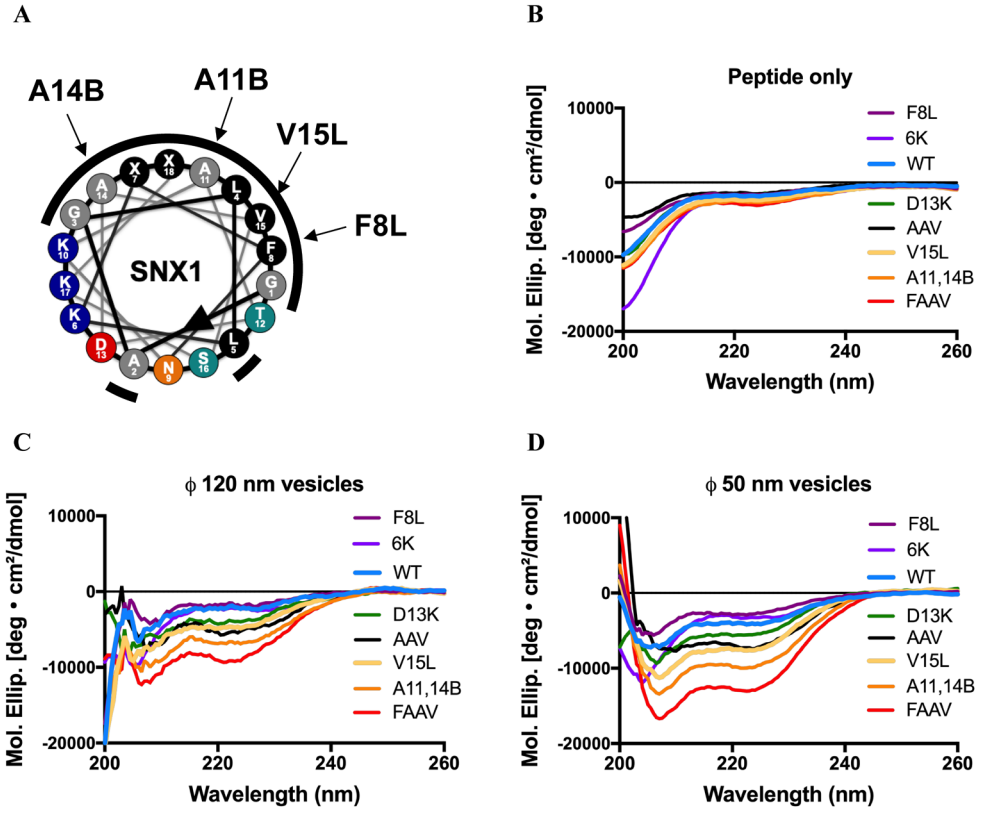

Fig. 3. Effects of Amino Acid Substitution on the Hydrophobic Face on the Improvement of α-Helicity

(A) A helical wheel projection of SNX1. Amino acids with highly and slightly hydrophobic side chains are shown in black and gray, respectively. Acidic and basic amino acids are colored in red and blue, respectively. Polar uncharged amino acids are indicated in orange (side chains with an amide group) or green (side chains with a hydroxy group). The black circular arc indicates the hydrophobic region. CD spectra of SNX1 WT and mutant peptides measured alone (B), or in the presence of lipid vesicles of 120 nm (C) and 50 nm (D). The standard lipid composition and unlabeled peptides were used ([L]/[P] ratio = 1000). (Color figure can be accessed in the online version.)

negatively charged lipids are required for both SNX1 and ARF to sense highly curved membranes such as 50 nm vesicles.

α-Helicity Was Increased by Substitution of Amino Acids Close to the Hydrophobic Face of the Amphiphilic Helix Several helices in proteins involved in curvature response are reported to be disordered structures in solution but to fold following membrane insertion.[8,13] SNX1 exhibited the highest curvature recognition (Fig. 1) and an α-helical structure in the presence of lipid vesicles (Supplementary Fig. S1). We expected that the α-helical structure to play a vital role in membrane-curvature recognition, and improvement of the α-helicity of SNX1 by mutation was directly connected to enhanced curvature recognition. The helix wheel projection of SNX1 is shown in Fig. 3A. Hydrophobic and hydrophilic residues are shown in gray and color, respectively (Gly and Ala residues were categorized into the former group in this study). Some residues close to the hydrophobic face were replaced with other residues expected to improve the α-helicity of SNX1. The Phe residue at the position 8 and Val residue at the position 15 were each mutated to Leu, respectively (F8L and V15L), which is found at relatively high frequency in α-helical structures.[28,29] Although Ala residues are common in α-helical structures,[28,29] to increase the hydrophobicity of the hydrophobic face, the two Ala residues at the positions 11 and 14 were replaced with a non-proteogenic amino acid, 2-aminoisobutyric acid (Aib, B) (A11,14B). A quadruple mutant including all four substitutions (F8L, A11B, A14B, and V15L) was also generated (FAAV). Because Lys residues are also well found in α-helices, the Asp residue at the position of 13 was substituted with Lys (D13K). The concept of the mutant with three Lys residues on both N and C-termini (6K) was different from the others. As shown in Fig. 2, negatively charged lipids were suggested to be important for curvature sensing. Improvement of the interaction with negatively charged lipids was, therefore, expected to cause the peptide to accumulate on the membranes and to contribute to an increase in the α-helicity of SNX1 following insertion into the membrane. The sequences of the mutants and wild type (WT) of SNX1 are shown on Table 2. Vesicles with the standard lipid composition were used in this experiment ([L]/[P] ratio = 1000).

Table 2. Sequences of SNX1 WT and the Derived Mutants[a)]

Peptide	Sequence (X = Norleucine, B = 2-Aminoisobutyric acid)
SNX1(WT)	GAGLLKXFNKATDAVSKX-GSGSK(NBD)-amide
F8L	GAGLLKX**L**NKATDAVSKX-GSGSK(NBD)-amide
V15L	GAGLLKXFNKATDA**L**SKX-GSGSK(NBD)-amide
A11,14B	GAGLLKXFNK**B**TD**B**VSKX-GSGSK(NBD)-amide
FAAV	GAGLLKX**L**NK**B**TD**BL**SKX-GSGSK(NBD)-amide
AAV	GAGLLKXFNK**B**TD**BL**SKX-GSGSK(NBD)-amide
D13K	GAGLLKXFNKAT**K**AVSKX-GSGSK(NBD)-amide
6K	**KKK**-GAGLLKXFNKATDAVSKX-**KKK**-GSGSK(NBD)-amide

a) In the peptide sequence, the single letters X and B in the sequences represent norleucine and 2-aminoisobutyric acid, respectively.

While all peptides alone showed random coil structures (Fig. 3B), they tended to adopt α-helix structures in the presence of vesicles (Fig. 3C, D). The α-helicities of the peptides

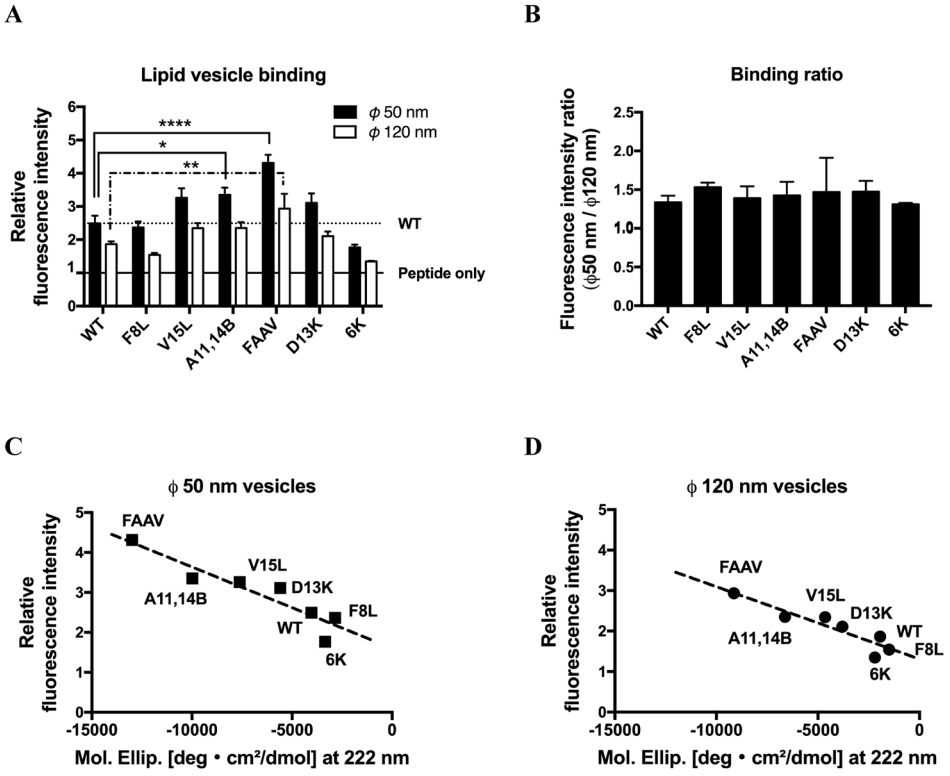

Fig. 4. Correlation between Lipid Vesicle Binding and the α-Helicity

(A) Comparison of the RFI values of SNX1-derived peptides in the presence of 50 nm (black) or 120 nm (white) lipid vesicles. The fluorescence intensity of peptides alone (Peptide only) and the RFI value of WT in the presence of 50 nm vesicles (WT) are indicated by horizontal solid and dashed lines, respectively. The data represent mean ± S.E. ($n = 3$). Statistical significance was determined using the two-way ANOVA Donnett's multiple comparisons test, with $\alpha = 0.05$ (Prism 7, ver. 7.0a software). (B) Comparison of curvature sensitivity. The fluorescence intensity of each peptide in the presence of 50 nm vesicles was divided by that in the presence of 120 nm vesicles. RFI values (Fig. 4A) are plotted against the molar ellipticities at 222 nm (Figs. 3C, D) of peptides in the presence of 50 nm (C) and 120 nm vesicles (D).

incubated with 50 nm vesicles increased more than in those incubated with 120 nm vesicles (Figs. 3C, D). This suggested that the peptides were induced to form α-helix structures from random coil structures to accommodate the lipid-packing defects upon binding to vesicles. In particular, FAAV showed the highest α-helicity among the peptides in the presence of vesicles. By contrast, the α-helicity of F8L and 6K decreased compared to the WT (Fig. 3D). We also made a triple mutation variant (AAV) with A11B, A14B, and V15L but not F8L. Because the F8L single mutation did not contribute to improvement of the α-helicity (Figs. 3C, D), the substitution was not expected to be required for FAAV. However, interestingly, against expectation AAV exhibited much lower α-helicity than FAAV in the presence of both 50 and 120 nm vesicles (Figs. 3C, D). These results indicated that the four mutations located on the hydrophobic face have a synergistic effect on α-helicity improvement. Although the substitution of amino acids close to the hydrophobic face contributed to the increased α-helicity, that of the FAAV peptide was still not very high [$[\theta]_{222}$ in the presence of 50 nm vesicles: $-13000\,\mathrm{deg\,cm^2/dmol}$]. While the substitution of SNX1 is a good case study, to better enhance the α-helicity, another peptide designs might be necessary (*cf.* the "Discussion").

Lipid Vesicle Binding Is Closely Correlated with Peptide α-Helicity We next examined the relationship between α-helicity and lipid vesicle binding. Figure 4A shows the RFI values of the SNX1-derived peptides incubated with 50 nm vesicles compared with that of WT (dotted line). Lipid vesicles with the standard lipid composition were used, and the [L]/[P] ratio was fixed at 1000. A11,14B and FAAV mutants with high α-helicity showed higher RFI values than that of WT in the presence of 50 nm vesicles (Fig. 4A, black bars). By contrast, the RFI values of F8L and 6K mutants with low α-helicity were the same or lower than that of WT. A similar tendency was seen in the peptides incubated with 120 nm vesicles (white bars). When plotting RFI values against the molar ellipticities at 222 nm, good correlations between them were observed in the SNX1 derivatives incubated with either 50 nm or 120 nm vesicles (Figs. 4C, D). Additionally, no disruption of lipid vesicles was confirmed by the leakage assay under the above experimental conditions ([L]/[P] ratio of 1000) (Supplementary Fig. S2). A fluorescent dye, ANTS, was enclosed in lipid vesicles with a quencher reagent, DPX, and fluorescent recovery of ANTS would be observed if the vesicle membrane was disrupted in the presence of the peptides. The leakage of ANTS was not recognized under the conditions of [L]/[P] ratios $\geq$100 regardless of the vesicle size (black bars), as the fluorescence intensities remained at the same level as the no-peptide condition (described as "Vesicle only"). As a control, when the same samples were treated with a detergent reagent, Triton X-100, after incubation with peptides, a rise in the fluorescence of ANTS was observed (white bars). The leakage of ANTS was observed only for the [L]/[P] ratio of 10, and no further increase in the fluorescence was observed even following Triton X-100 treatment. The above results indicated that an increase in the α-helicity of curvature-sensing peptides is a crucial factor for the improvement of lipid vesicle binding. However, since fluorescence intensity ratios between the

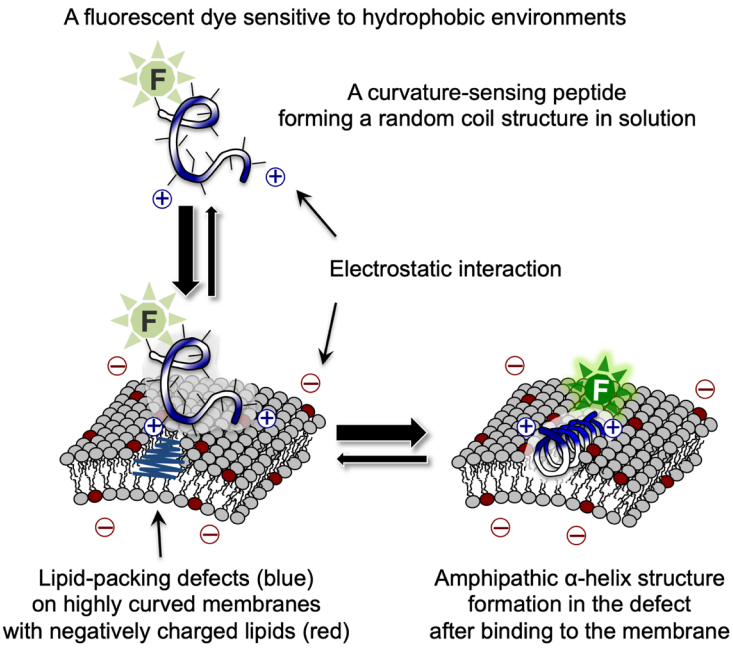

Fig. 5. A Proposed Sensing Model for High Curvature Membranes

A curvature-sensing peptide forms a random coil structure in solution, and the hydrophobic environment-sensitive dye (shown as "F") conjugated with the peptide emits weak fluorescence. The blue and white colors on the peptide indicate positively charged regions and hydrophobic regions, respectively. The electrostatic interaction between the positively charged residues and negatively charged lipids is one of important factors for the membrane approach of the peptide. There are numerous lipid-packing defects on highly curved membranes, and the curvature-sensing peptide possibly recognizes these defects and forms an amphipathic α-helix structure to accommodate the size of the defect. At that time, the NBD dye emits strong fluorescence under the hydrophobic condition. By introducing mutations into the peptide to form an amphipathic α-helix structure, binding to the membrane defects becomes more stable. (Color figure can be accessed in the online version.)

presences of 50 nm vesicles and 120 nm vesicles were similar for each peptide (Figs. 4A, B), it appeared that increased α-helicity did not contribute to the curvature sensitivity. To improve the ability more detailed investigation is required in the future work.

Discussion

Based on a structure–activity correlation study, we developed a SNX1 derivative peptide FAAV, which is expected to be a promising curvature-sensing peptide prototype. Mutations of the amino acids close to the hydrophobic face, clearly demonstrated that improvement of α-helix formation is closely correlated with an increase in lipid binding ability (Figs. 4C, D). In a possible binding model (Fig. 5), the correlation is attributed to the fact that the α-helix formation is required to accommodate to the lipid-packing defects on the membranes. To better improve the lipid vesicle binding ability, additional modifications of FAAV would be required to further increase the α-helicity. For example, a hydrocarbon-stapling between amino acids at the positions of i and $i+4$ or i and $i+7$ forces a peptide to form an α-helical structure. Stapling compensates for entropy loss during occurring on the conformational change from a random coil to an α-helix and is expected to contribute to the improvement of the binding ability to highly curved membranes. Another strategy is to conjugate FAAV with compounds enriched in hydrophobicity such as long-chain fatty acids or cholesterol as an anchoring unit to increase the affinity for the membranes.

Surprisingly, the electrostatic interaction between negatively charged lipids and the positively charged residues of the peptides was responsible for curvature sensing (Fig. 2). The mechanism underlying curvature recognition by the peptides is still under the debate. One plausible explanation for this phenomenon is that at the initial step the peptides require an electrostatic interaction to approach to the lipid vesicle; another is that after binding to the lipid surface the negatively charged lipids help the peptides maintain stable binding to the vesicles. In any case, it needs to pursue the exact factors causing the curvature recognition in the future work.

Amphipathic helical peptides with a wide hydrophobic face may be suitable for sensing membrane curvature. Peptides that showed relatively high curvature sensing abilities, such as SNX1, SNX2, and ARF, tended to have wide hydrophobic faces that occupy the half of the amphipathic helices (Supplementary Fig. S3). This propensity is also seen in the part of the ALPS motif that has an amphipathic helix[8] (Supplementary Fig. S3). By contrast, the other peptides with relatively low curvature sensing abilities had narrow hydrophobic faces (Supplementary Fig. S3). The curvature-inducing peptide, EpN18, has a hydrophobic face of one-third the size of the entire helical wheel.[4,5]

FAAV has several advantages that differentiate it from previously reported curvature-sensing peptides, such as MARCKS-ED and the ALPS motif. FAAV has a greater lipid vesicle-binding ability than MARCKS-ED, evidenced by the fact that WT SNX1 showed an equal or higher RFI value compared to MARCKS-ED (Fig. 1), and FAAV had a greater binding ability than WT (Fig. 4A). While MARCKS-ED does not have any secondary structure in the presence of vesicles,[7] our peptide, FAAV, adopts an amphipathic α-helical structure (Fig. 3). The vesicle binding ability of the former peptide is influenced by the positions and numbers of both positively charged residues and hydrophobic residues,[9] while the ability of the latter one is dependent on its propensity for

α-helix formation. Due to these differences, the approaches for modifying these peptides to improve their curvature sensing are inevitably distinct. By contrast, ALPS motif shares two similarities with FAAV as following: (*i*) both are unstructured in solution but form an amphipathic helix on highly curved membranes, and (*ii*) both have a wide hydrophobic face that occupies almost half of the amphipathic helix. FAAV is composed of 23 a.a. including the liker segment, and is generally shorter in chain length than peptides containing an ALPS motif. This feature may provide advantages over the ALPS motif in ease of sample preparation, design, and biological development.

Conclusion

In this study, we generated a novel membrane curvature-sensing peptide, FAAV, as a prototype curvature sensor. In screening experiments of the initial peptides, SNX1 was found to be the most sensitive to membrane curvature among 11 candidate peptides predicted to form an amphipathic α-helical structure. We also demonstrated the importance of negatively charged lipids for vesicle binding of the peptides. SNX1 had negatively charged lipid-sensing abilities in addition to its curvature-sensing ability. We found a close correlation between α-helicity and lipid vesicle binding. A SNX1 derivative mutant, FAAV, which adopts an amphipathic α-helical structure, was superior to the other peptides examined for vesicle binding abilities. The peptides designed in the present study have the potential to serve as prototype tools for the visualization of various biological phenomena. Future works will focus on improving the target specificity and binding affinity of membrane-curvature recognition tools.

Acknowledgments This work was supported by JSPS KAKENHI Grant JP18H04547 (S.F.) and the Takeda Science Foundation (K.K.).

Conflict of Interest The authors declare no conflict of interest.

Supplementary Materials The online version of this article contains supplementary materials.

References

1) Zhao Y., Liu J., Yang C., Capraro B. R., Baumgart T., Bradley R. P., Ramakrishnan N., Xu X., Radhakrishnan R., Svitkina T., Guo W., *Dev. Cell*, **26**, 266–278 (2013).
2) Lou H. Y., Zhao W., Zeng Y., Cui B., *Acc. Chem. Res.*, **51**, 1046–1053 (2018).
3) Sugiura Y., Ikeda K., Nakano M., *Langmuir*, **31**, 11549–11557 (2015).
4) Pujals S., Miyamae H., Afonin S., Murayama T., Hirose H., Nakase I., Taniuchi K., Umeda M., Sakamoto K., Ulrich A. S., Futaki S., *ACS Chem. Biol.*, **8**, 1894–1899 (2013).
5) Murayama T., Masuda T., Afonin S., Kawano K., Takatani-Nakase T., Ida H., Takahashi Y., Fukuma T., Ulrich A. S., Futaki S., *Angew. Chem. Int. Ed. Engl.*, **56**, 7644–7647 (2017).
6) Simunovic M., Voth G. A., Callan-Jones A., Bassereau P., *Trends Cell Biol.*, **25**, 780–792 (2015).
7) Morton L. A., Yang H., Saludes J. P., Fiorini Z., Beninson L., Chapman E. R., Fleshner M., Xue D., Yin H., *ACS Chem. Biol.*, **8**, 218–225 (2013).
8) Bigay J., Casella J. F., Drin G., Mesmin B., Antonny B., *EMBO J.*, **24**, 2244–2253 (2005).
9) de Jesus A. J., White O. R., Flynn A. D., Yin H., *Biophys. J.*, **110**, 1980–1992 (2016).
10) Peter B. J., Kent H. M., Mills I. G., Vallis Y., Butler P. J., Evans P. R., McMahon H. T., *Science*, **303**, 495–499 (2004).
11) Bhatia V. K., Madsen K. L., Bolinger P. Y., Kunding A., Hedegard P., Gether U., Stamou D., *EMBO J.*, **28**, 3303–3314 (2009).
12) Chen Z., Zhu C., Kuo C. J., Robustelli J., Baumgart T., *J. Am. Chem. Soc.*, **138**, 14616–14622 (2016).
13) Gallop J. L., Jao C. C., Kent H. M., Butler P. J., Evans P. R., Langen R., McMahon H. T., *EMBO J.*, **25**, 2898–2910 (2006).
14) Hatzakis N. S., Bhatia V. K., Larsen J., Madsen K. L., Bolinger P. Y., Kunding A. H., Castillo J., Gether U., Hedegard P., Stamou D., *Nat. Chem. Biol.*, **5**, 835–841 (2009).
15) Galic M., Jeong S., Tsai F. C., Joubert L. M., Wu Y. I., Hahn K. M., Cui Y., Meyer T., *Nat. Cell Biol.*, **14**, 874–881 (2012).
16) Herlo R., Lund V. K., Lycas M. D., Jansen A. M., Khelashvili G., Andersen R. C., Bhatia V., Pedersen T. S., Albornoz P. B. C., Johner N., Ammendrup-Johnsen I., Christensen N. R., Erlendsson S., Stoklund M., Larsen J. B., Weinstein H., Kjaerulff O., Stamou D., Gether U., Madsen K. L., *Cell Reports*, **23**, 2056–2069 (2018).
17) Vanoosthuyse V., Tichtinsky G., Dumas C., Gaude T., Cock J. M., *Plant Physiol.*, **133**, 919–929 (2003).
18) van Weering J. R., Sessions R. B., Traer C. J., Kloer D. P., Bhatia V. K., Stamou D., Carlsson S. R., Hurley J. H., Cullen P. J., *EMBO J.*, **31**, 4466–4480 (2012).
19) Kosuge M., Takeuchi T., Nakase I., Jones A. T., Futaki S., *Bioconjug. Chem.*, **19**, 656–664 (2008).
20) Strahilevitz J., Mor A., Nicolas P., Shai Y., *Biochemistry*, **33**, 10951–10960 (1994).
21) Kawaguchi Y., Takeuchi T., Kuwata K., Chiba J., Hatanaka Y., Nakase I., Futaki S., *Bioconjug. Chem.*, **27**, 1119–1130 (2016).
22) Habermann B., *EMBO Rep.*, **5**, 250–255 (2004).
23) Fukasawa M., Nishijima M., Itabe H., Takano T., Hanada K., *J. Biol. Chem.*, **275**, 34028–34034 (2000).
24) Connor J., Bucana C., Fidler I. J., Schroit A. J., *Proc. Natl. Acad. Sci. U.S.A.*, **86**, 3184–3188 (1989).
25) Utsugi T., Schroit A. J., Connor J., Bucana C. D., Fidler I. J., *Cancer Res.*, **51**, 3062–3066 (1991).
26) Birge R. B., Boeltz S., Kumar S., Carlson J., Wanderley J., Calianese D., Barcinski M., Brekken R. A., Huang X., Hutchins J. T., Freimark B., Empig C., Mercer J., Schroit A. J., Schett G., Herrmann M., *Cell Death Differ.*, **23**, 962–978 (2016).
27) Record M., Carayon K., Poirot M., Silvente-Poirot S., *Biochim. Biophys. Acta*, **1841**, 108–120 (2014).
28) Fujiwara K., Toda H., Ikeguchi M., *BMC Struct. Biol.*, **12**, 18 (2012).
29) Pace C. N., Scholtz J. M., *Biophys. J.*, **75**, 422–427 (1998).